

Effects of Fermi surface and superconducting gap structure in the field-rotational experiments: A possible explanation of the cusp-like singularity in $\text{YNi}_2\text{B}_2\text{C}$

Masafumi Udagawa, Youichi Yanase, and Masao Ogata
Department of Physics, University of Tokyo, Hongo, Tokyo 113-0033, Japan
 (Dated: September 25, 2018)

We have studied the field-orientational dependence of zero-energy density of states (FODOS) for a series of systems with different Fermi surface and superconducting gap structures. Instead of phenomenological Doppler-shift method, we use an approximate analytical solution of Eilenberger equation together with self-consistent determination of order parameter and a variational treatment of vortex lattice. First, we compare zero-energy density of states (ZEDOS) when a magnetic field is applied in the nodal direction ($\nu_{\text{node}}(0)$) and in the antinodal direction ($\nu_{\text{anti}}(0)$), by taking account of the field-angle dependence of order parameter. As a result, we found that there exists a crossover magnetic field H^* so that $\nu_{\text{anti}}(0) > \nu_{\text{node}}(0)$ for $H < H^*$, while $\nu_{\text{node}}(0) > \nu_{\text{anti}}(0)$ for $H > H^*$, consistent with our previous analyses. Next, we showed that H^* and the shape of FODOS are determined by contribution from the small part of Fermi surface where Fermi velocity is parallel to field-rotational plane. In particular, we found that H^* is lowered and FODOS has broader minima, when a superconducting gap has point nodes, in contrast to the result of the Doppler-shift method. We also studied the effects of in-plane anisotropy of Fermi surface. We found that in-plane anisotropy of quasi-two dimensional Fermi surface sometimes becomes larger than the effects of Doppler-shift and can destroy the Doppler-shift predominant region. In particular, this tendency is strong in a multi-band system where superconducting coherence lengths are isotropic. Finally, we addressed the problem of cusp-like singularity in $\text{YNi}_2\text{B}_2\text{C}$ and present a possible explanation of this phenomenon.

PACS numbers:

I. INTRODUCTION

While it is accepted that electron correlation drives non-s-wave-pairing superconductivity, determination of detailed superconducting gap structure still remains a challenge for both theory and experiment. On a theoretical side, analyses starting at microscopic Hamiltonians have succeeded in identifying gap structures of several materials. On an experimental side, it is getting recognized that field-orientational dependence of specific heat or thermal conductivity carries a considerable information on gap structure. Since the low-energy density of states changes according to the angle between gap nodes and magnetic field, one can derive gap structure by tracing a change of thermodynamic quantities as sweeping magnetic field in several directions. Actually, this method has been applied to a series of superconductors including Sr_2RuO_4 ^{1,2,3,4}, CeCoIn_5 ^{5,6}, $\kappa-(\text{ET})_2\text{Cu}(\text{NCS})_2$ ⁷, $\text{YNi}_2\text{B}_2\text{C}$ ^{8,9}, $\text{PrOs}_4\text{Sb}_{12}$ ¹⁰ and UPd_2Al_3 ¹¹. However, their results left serious problems yet to be overcome. For example, in the case of Sr_2RuO_4 , thermal conductivity (κ) does not show any change with rotating magnetic field within the ab-plane, while specific heat (C) shows clear four-fold oscillation. As to CeCoIn_5 , κ and C show incompatible behavior. In $\text{YNi}_2\text{B}_2\text{C}$, both κ and C show a cusp-like singularity as sweeping magnetic field within the superconducting plane.

In the previous paper, we addressed the problem of Sr_2RuO_4 in terms of the fine-structure of density of states¹². Whereas, the latter two problems are left unsolved. While it is proposed that the cusp-like singularity in $\text{YNi}_2\text{B}_2\text{C}$ is caused by point node in gap structure¹³,

their discussion is phenomenological in nature and unreliable, as we will show.

The confusion as to the experiment is probably attributed to a lack of firm theoretical basis. So far, the experimental data has been usually interpreted in terms of the ‘‘Doppler-shift criterion’’. This criterion says *larger density of states is obtained when a magnetic field is applied in antinodal rather than nodal directions*. However, this criterion is obtained on the basis of the phenomenological Doppler-shift method that can be justified only at a limit of low-magnetic field. Hence, it is not clear whether this criterion is still valid in the experimentally accessible higher magnetic fields.

In fact, in the previous paper, we showed that there occurs a crossover from Doppler-shift predominant region at low magnetic fields to core states predominant region at high magnetic fields¹². In the core state predominant region, larger density of states is obtained for field in nodal direction, in contrast to the ‘‘Doppler-shift criterion’’. Hence, in order to derive a correct nodal structure from the field-rotational experiments, it is highly desirable to establish a theoretical analysis applicable more widely.

To this end, we present a more quantitative analyses of the crossover behavior by taking account of the field-angle dependence of order parameter. In particular, we are interested in how the Fermi surface or superconducting gap structures affect the crossover behavior.

Furthermore, we would like to investigate field-orientational dependence of zero-energy density of states (FODOS) in detail at the Doppler-shift predominant region. It is interesting to clarify how information on nodal

structure is obtained from the shape of FODOS.

The structure of this paper is as follows. In the next section, we summarize our method. In section III, we present a quantitative study of the crossover behavior for several models with different Fermi surface and nodal structures. In section IV, we examine the effects of in-plane anisotropy of Fermi surface to the crossover behavior. In section V we address the problem of cuspsingularity in $\text{YNi}_2\text{B}_2\text{C}$. And section VI is devoted to conclusions.

II. METHOD

In this section, we introduce an approximate analytical solution of the quasiclassical Eilenberger equation, which was originally proposed by Pesch¹⁴, and recently extended to unconventional superconductors by Dahm et al.¹⁵. With this method, one can obtain exact results at $H = H_{c2}$, and quantitatively reliable results to much lower fields. All our analyses in this paper are based on this approximate analytical approach.

We start with the quasiclassical Eilenberger equation^{19,20}. This equation provides a convenient method to analyze inhomogeneous state of superconductors by decoupling slowly varying order parameter from fast oscillating Fermi-particle degree of freedom. In this paper, we limit ourselves to the case of spin-singlet superconductors in clean limit. Under these conditions, the quasiclassical Eilenberger equations read

$$\mathbf{v}_F \cdot (\nabla - i\frac{2e}{c}\mathbf{A}(\mathbf{r}))f + 2\omega_n f - 2i\Delta g = 0, \quad (1)$$

$$\mathbf{v}_F \cdot (\nabla + i\frac{2e}{c}\mathbf{A}(\mathbf{r}))f^\dagger - 2\omega_n f^\dagger + 2i\Delta^* g = 0, \quad (2)$$

with the normalization condition

$$g^2 - f f^\dagger = 1. \quad (3)$$

Here, $g = g(\mathbf{r}, \mathbf{k}_F, i\omega_n)$, $f = f(\mathbf{r}, \mathbf{k}_F, i\omega_n)$ and $f^\dagger = f^\dagger(\mathbf{r}, \mathbf{k}_F, i\omega_n)$ are normal and anomalous components of quasiclassical Green function, $\omega_n = (2n+1)\pi T$ is Matsubara frequency, and $\Delta = \Delta(\mathbf{r}, \mathbf{k}_F)$ denotes order parameter. The order parameter Δ is determined in a self-consistent way, by solving the following gap equation.

$$\Delta(\mathbf{r}, \mathbf{k}_F) = -2\pi i T \nu_n(0) \sum_{0 < \omega_n < \omega_c} \langle V(\mathbf{k}_F, \mathbf{k}'_F) \times f(\mathbf{r}, \mathbf{k}'_F, i\omega_n) \rangle_{FS(\mathbf{k}'_F)}. \quad (4)$$

Here, $\nu_n(0) = \int_{FS} \frac{d\Omega}{v_F}$ is Zero-energy density of states (ZEDOS) in the normal state, ω_c , a cut-off energy, $V(\mathbf{k}_F, \mathbf{k}'_F)$, a pairing potential. and $\langle \dots \rangle_{FS}$ means taking average on the Fermi surface, namely, $\langle \dots \rangle_{FS} = \frac{\int_{FS} \frac{d\Omega}{\nu_n(0)} \frac{1}{v_F} \dots$.

Free energy Ω_s can also be expressed with the quasiclassical Green function in a closed form^{19,21}.

$$\Omega_s - \Omega_n = \int d\mathbf{r} \frac{(\mathbf{B} - \mathbf{H})^2}{8\pi} + \pi i T \nu_n(0) \times \sum_{0 < \omega_n < \omega_c} \langle \frac{g+1}{g-1} (\Delta^* f + \Delta f^\dagger) \rangle_{FS}, \quad (5)$$

with Ω_n , free energy in the normal state, \mathbf{H} , external magnetic field, and \mathbf{B} , total magnetic field. Equations (1)-(5) form a basis to study inhomogeneous superconductors.

Next, we introduce an approximate analytical solution of Eilenberger equation. Equations (1)-(3) can be solved analytically only at $H = H_{c2}$. However, by extending the analytical solution to lower fields, one can obtain quantitatively reliable results for density of states etc, well below H_{c2} . To obtain approximate analytical solution at arbitrary fields, we have to make three assumptions which are exactly justified at $H = H_{c2}$.

First, we decouple the order parameter into the spatial and momentum parts

$$\Delta(\mathbf{r}, \mathbf{k}_F) = \Delta_0 \Psi(\mathbf{r}) \Phi(\mathbf{k}_F), \quad (6)$$

and normalize $\Psi(\mathbf{r})$ and $\Phi(\mathbf{k}_F)$ as

$$\langle |\Psi(\mathbf{r})|^2 \rangle_{\mathbf{r}} = 1, \quad (7)$$

$$\langle |\Phi(\mathbf{k}_F)|^2 \rangle_{FS} = 1. \quad (8)$$

Here, $\langle \dots \rangle_{\mathbf{r}}$ means averaging in the real space. If $\Psi(\mathbf{r})$ is periodic, this is equivalent to taking average over a unit cell. Then, we assume the spatial variation $\Psi(\mathbf{r})$ is described by Abrikosov vortex function, namely,

$$\Psi(\mathbf{r}) = \Psi_A(\mathbf{r}) = \frac{1}{N} \sum_{n=-\infty}^{\infty} \exp \left[2\pi i n \frac{y - \frac{n+1}{2} y_1}{y_0} - \frac{\pi \delta}{\Lambda} (x - n x_0)^2 \right]. \quad (9)$$

$\Psi_A(\mathbf{r})$ can be obtained by solving linearized Ginzburg-Landau equation with different coherence lengths in x (ξ_x) and in y (ξ_y) directions. Here, we set x and y axes perpendicular to the magnetic field. $N = (\frac{y_0}{2x_0\delta})^{\frac{1}{4}}$ is a normalization constant to make $\langle |\Psi(\mathbf{r})|^2 \rangle_{\mathbf{r}} = 1$. Area of unit cell, Λ , can be related to the total magnetic field B by

$$\Lambda = x_0 y_0 = \frac{\pi c}{eB}. \quad (10)$$

δ denotes the anisotropy of superconducting coherence lengths, i.e., $\delta = \frac{\xi_y}{\xi_x}$. One can estimate δ to be $\delta \sim$

$\sqrt{\frac{\langle v_{Fy}^2 \rangle}{\langle v_{Fx}^2 \rangle}}$ for single-band superconductors.

Here we note that $\Psi(\mathbf{r})$ denotes an Abrikosov vortex lattice which is spanned by two lattice vectors, $(0, y_0)$ and

(x_0, y_1) . When $y_1 = 0$, $\Psi(\mathbf{r})$ describes a square (rectangular) lattice, while when $y_1 = \frac{y_0}{2}$, $\Psi(\mathbf{r})$ describes a triangular lattice. However, the shape of the unit cell is unimportant in the subsequent analyses.

As a second assumption, we set Ginzburg-Landau parameter κ to be much larger than 1, hence $\mathbf{B} = \mathbf{H}$. This assumption is justified for a lot of unconventional superconductors including $\text{YNi}_2\text{B}_2\text{C}$.

The third assumption is that we ignore spatial fluctuation of $g(\mathbf{r}, \mathbf{k}_F, i\omega_n)$, namely, $\langle g^2 \rangle_{\mathbf{r}} = \langle g \rangle_{\mathbf{r}}^2$. Since at $H = H_{c2}$, the order parameter vanishes and translational symmetry is recovered, this assumption is also justified. The validity of this assumption has been justified for lower fields¹⁵.

With these three assumptions, one can obtain an approximate analytical solution of eqs. (1)-(3) at arbitrary magnetic fields by utilizing the operator techniques introduced in ref. 22. We summarize the basic results below. For details, see, for example, refs. 15 and 16.

[1] spatial average of $g(\mathbf{r}, \mathbf{k}_F, i\omega_n)$

$$\langle g(\mathbf{r}, \mathbf{k}_F, i\omega_n) \rangle_{\mathbf{r}} = -\text{Re} \frac{1}{\sqrt{1 + P(\mathbf{v}_F, i\omega_n)}}, \quad (11)$$

where,

$$P(\mathbf{v}_F, i\omega_n) = \frac{4\Lambda}{\pi} |\Delta_0|^2 \left(\frac{|\Phi(\mathbf{k}_F)|}{|\mathbf{v}_{F\perp}|} \right)^2 (1 - F(\Lambda, \mathbf{v}_{F\perp}, \omega_n)), \quad (12)$$

$$F(\Lambda, \mathbf{v}_{F\perp}, \omega_n) = \int_0^\infty du \exp\left(-u - \frac{\pi |\mathbf{v}_{F\perp}|^2}{8\Lambda\omega_n^2} u^2\right). \quad (13)$$

Here, effective Fermi velocity $\mathbf{v}_{F\perp}$ is expressed as

$$\mathbf{v}_{F\perp} = \sqrt{\delta} v_{Fx} \mathbf{e}_x + \frac{1}{\sqrt{\delta}} v_{Fy} \mathbf{e}_y, \quad (14)$$

with the projection of Fermi velocity on x (v_{Fx}) and y (v_{Fy}) axes.

[2] DOS $\nu(\epsilon)$

$$\frac{\nu(\epsilon)}{\nu_n(0)} = -\langle \langle g(\mathbf{r}, \mathbf{k}_F, i\omega_n \rightarrow \epsilon + i0) \rangle_{\mathbf{r}} \rangle_{FS}. \quad (15)$$

In particular, the formula of ZEDOS becomes quite simple.

$$\frac{\nu(0)}{\nu_n(0)} = \langle \frac{1}{\sqrt{1 + \frac{4\Lambda}{\pi} |\Delta_0|^2 \left(\frac{|\Phi(\mathbf{k}_F)|}{|\mathbf{v}_{F\perp}|} \right)^2}} \rangle_{FS}. \quad (16)$$

[3] gap equation

In order to obtain gap equation, we decouple $V(\mathbf{k}_F, \mathbf{k}'_F)$ as $V(\mathbf{k}_F, \mathbf{k}'_F) = V\Phi^*(\mathbf{k}_F)\Phi(\mathbf{k}'_F)$, then

we obtain

$$\log\left(\frac{2e^\gamma \omega_c}{\pi T_c}\right) = \sum_{0 < \omega_n < \omega_c} \frac{2\pi T_c}{\omega_n} < |\Phi(\mathbf{k}_F)|^2 \times \frac{F(\Lambda, \mathbf{v}_{F\perp}, \omega_n)}{\sqrt{1 + P(\mathbf{v}_F, i\omega_n)}} >_{FS}, \quad (17)$$

where $\gamma = 0.5772 \dots$ is Euler's constant. The formula to determine H_{c2} can be obtained by setting $\Delta_0 = 0$ in eq. (17).

$$\log\left(\frac{2e^\gamma \omega_c}{\pi T_c}\right) = \int_0^\infty ds \frac{1 - \exp(-\frac{\omega_c s}{\pi T})}{\sinh s} < |\Phi(\mathbf{k}_F)|^2 \times e^{-\frac{|\mathbf{v}_{F\perp}|^2}{8\pi T^2 \Lambda} s^2} >_{FS}. \quad (18)$$

[4] free energy

$$\Omega_s - \Omega_n = -\nu_n(0) |\Delta_0|^2 \sum_{0 < \omega_n < \omega_c} \frac{2\pi T_c}{\omega_n} < |\Phi(\mathbf{k}_F)|^2 \times \frac{P(\mathbf{v}_F, i\omega_n) F(\Lambda, \mathbf{v}_{F\perp}, \omega_n)}{\sqrt{1 + P(\mathbf{v}_F, i\omega_n)} (1 + \sqrt{1 + P(\mathbf{v}_F, i\omega_n)})^2} >_{FS}. \quad (19)$$

We calculate density of states by the following procedure. First, Fermi velocity \mathbf{v}_F and nodal structure $\Phi(\mathbf{k}_F)$ are determined by assuming a phenomenological model or starting at a microscopic Hamiltonian. Then, at a given temperature T and a magnetic field \mathbf{H} , one can calculate order parameter amplitude Δ_0 by solving eq. (17). By substituting Δ_0 into eq. (15), one can obtain DOS $\nu(\epsilon)$. When magnetic field is applied off a symmetry axis, the ratio of coherence lengths δ deviates from 1. In this case, we determine δ variationally by minimizing free energy eq. (19) with respect to δ . This prescription is equivalent to the variational ansatz of Abrikosov vortex lattice introduced in refs. 16 and 23.

One can incorporate multi-band properties into this approximate analytical approach with a slight modification of [1]-[4]^{16,17}. In multi-band systems, \mathbf{k}_F , \mathbf{v}_F , f , f^\dagger , g , Δ , $\nu_n(0)$ become band-dependent. To specify band index, we write these quantities as \mathbf{k}_F^α , \mathbf{v}_F^α , f^α , $f^{\alpha\dagger}$, g^α , Δ^α , $\nu_n^\alpha(0)$. Next, we decouple order parameter as

$$\Delta^\alpha(\mathbf{r}, \mathbf{k}_F^\alpha) = \Delta_0^\alpha \Psi^\alpha(\mathbf{r}) \Phi^\alpha(\mathbf{k}_F^\alpha). \quad (20)$$

Here, we assume $\Psi^\alpha(\mathbf{r})$ to be described by Abrikosov lattice, $\Psi_A(\mathbf{r})$. Furthermore, we assume that the anisotropy of coherence lengths δ^α are the same for all bands ($\delta^\alpha = \delta$), and determine δ by minimizing free energy. Due to inter-band mixing effect by a pair-hopping term, the spatial variation of Δ of each bands are not independent any longer. Then, one can take account of the inter-band mixing effect through minimization of δ .

As we will discuss in section. V, we are interested in a system where quasi-two-dimensional Fermi surface and three-dimensional Fermi surface co-exist. In such a system, superconducting coherence length may be isotropic

due to the three-dimensional Fermi surface, and lead to isotropic vortex structure. In this case, one may expect unusual phenomena characteristic of multi-band system, in the sense that quasi-two-dimensional Fermi surface and isotropic vortex structure are incompatible in a single-band superconductor.

Here, we note that some complication may arise in vortex structure due to multi-band effects. For example, it is proposed that order parameter of different bands may have zero-points at different places. However, we believe our results will not be influenced by the detail of vortex structure and ignore them.

Here, let us check how [1]-[4] are modified in a multi-band case. [1]spatial average of $g(\mathbf{r}, \mathbf{k}_F, i\omega_n)$ also holds for multi-band systems, by making each quantity in eqs. (11)-(14) band-dependent. [2]DOS $\nu(\epsilon)$ and [4]free energy are also correct by making the quantities band-dependent, and summing over band indices in the right sides of eqs. (15), (16), and (19). Only gap equation in [3] needs substantial modification. In a multi-band system, we decouple pair potential $V^{\alpha\beta}(\mathbf{k}_F^\alpha, \mathbf{k}_F^\beta)$ as $V(\mathbf{k}_F^\alpha, \mathbf{k}_F^\beta) = V^{\alpha\beta} \Phi^*(\mathbf{k}_F^\alpha) \Phi(\mathbf{k}_F^\beta)$, then gap equation eq. (17) becomes

$$\Delta_0^\alpha \log\left(\frac{2e^\gamma \omega_c}{\pi T_c}\right) = \sum_\beta \nu_n^\beta(0) V^{\alpha\beta} \Delta_0^\beta \sum_{0 < \omega_n < \omega_c} \frac{2\pi T_c}{\omega_n} \times < |\Phi^\beta(\mathbf{k}_F^\beta)|^2 \frac{F^\beta(\Lambda, \mathbf{v}_{F\perp}^\beta, \omega_n)}{\sqrt{1 + P^\beta(\mathbf{v}_F^\beta, i\omega_n)}} >_{FS(\mathbf{k}_F^\beta)}, \quad (21)$$

III. QUANTITATIVE STUDY OF THE CROSSOVER BEHAVIOR

In this section, we present a quantitative study of the crossover behavior for the following three models. Below, we take \mathbf{e}_a , \mathbf{e}_b and \mathbf{e}_c as a right-handed orthonormal basis.

(a) line nodes on spherical Fermi surface

$$\mathbf{v}_F = v_F(\sin \theta \cos \phi \mathbf{e}_a + \sin \theta \sin \phi \mathbf{e}_b + \cos \theta \mathbf{e}_c). \quad (22)$$

$$\Phi(\mathbf{k}_F) = \sqrt{\frac{15}{4}} \sin^2 \theta \sin 2\phi. \quad (23)$$

(b) line nodes on cylindrical Fermi surface

$$\mathbf{v}_F = v_F(\cos \phi \mathbf{e}_a + \sin \phi \mathbf{e}_b + \epsilon \sin k_z \mathbf{e}_c). \quad (24)$$

$$\Phi(\mathbf{k}_F) = \sqrt{2} \sin 2\phi. \quad (25)$$

Here, ϵ gives a small c-axis dispersion. We set $\epsilon = 0.05$.

(c) point nodes on spherical Fermi surface

$$\mathbf{v}_F = v_F(\sin \theta \cos \phi \mathbf{e}_a + \sin \theta \sin \phi \mathbf{e}_b + \cos \theta \mathbf{e}_c). \quad (26)$$

$$\Phi(\mathbf{k}_F) = \sqrt{\frac{15}{19}} (1 - \sin^2 \theta \cos 4\phi). \quad (27)$$

These models are often used to approximate more complicated realistic materials. Hence, it is important to study the basic properties of these models in detail.

Throughout our paper, we specify the direction of magnetic field with two parameters θ_0 and ϕ_0 as

$$\mathbf{H} = H(\sin \theta_0 \cos \phi_0 \mathbf{e}_a + \sin \theta_0 \sin \phi_0 \mathbf{e}_b + \cos \theta_0 \mathbf{e}_c). \quad (28)$$

In principle, we fix $\theta_0 = 90^\circ$ and study the change of ZEDOS with varying ϕ_0 in this paper. In other words, we consider the ab-plane as a field-rotational plane. As to the three models above, $\phi_0 = 0^\circ$ and $\phi_0 = 45^\circ$ correspond to the cases where a magnetic field is applied in nodal direction and antinodal direction, respectively.

Here, we focus on ZEDOS at low temperatures, because universal behaviors are expected in this region. We note that some cares are necessary to discuss thermodynamic quantities at higher temperature, because DOS at high energies depend on the magnetic field direction quite differently from ZEDOS¹². Thus we fix $T = 0.1T_c$ and $\omega_c = 20\pi T_c$ throughout this section. At this temperature, ZEDOS well represents the thermodynamic properties of a system.

A. Crossover behavior of ZEDOS and order parameter

First, we consider ZEDOS when magnetic field is applied in the nodal direction ($\nu_{node}(0)$) and in the antinodal direction ($\nu_{anti}(0)$). In the previous paper¹², we showed that the Doppler-shift criterion is correct at low fields, while it is broken at high fields due to the quasi-particles propagating parallel to magnetic field. In the previous paper, we used an assumption that Δ_0 does not depend on field direction. In the present paper, we calculate ZEDOS with determining Δ_0 self-consistently. In general, Δ_0 changes as field direction varies. In particular, near H_{c2} , in-plane anisotropy of H_{c2} influences FODOS through the field-angle dependence of Δ_0 . Perhaps, the anisotropy of H_{c2} continues to affect FODOS to lower fields, and suppress the Doppler-shift predominant region. Hence, it is of interest to estimate how the field-angle dependence of Δ_0 modifies the crossover behavior.

In fig. 1, we show the FODOS for the three models introduced above. These show a similar crossover behavior with different crossover fields H^* . For $H < H^*$, $\nu_{anti}(0) > \nu_{node}(0)$, consistent with the ‘‘Doppler-shift criterion’’, while for $H > H^*$, $\nu_{node}(0) > \nu_{anti}(0)$. These results are consistent with our previous analyses¹². Since H_{c2} is smaller when field is in the nodal direction ($H \parallel n$) than in the antinodal direction ($H \parallel a$) in all the three cases, the anisotropy of H_{c2} generally supports the relation $\nu_{node}(0) > \nu_{anti}(0)$ at high fields.

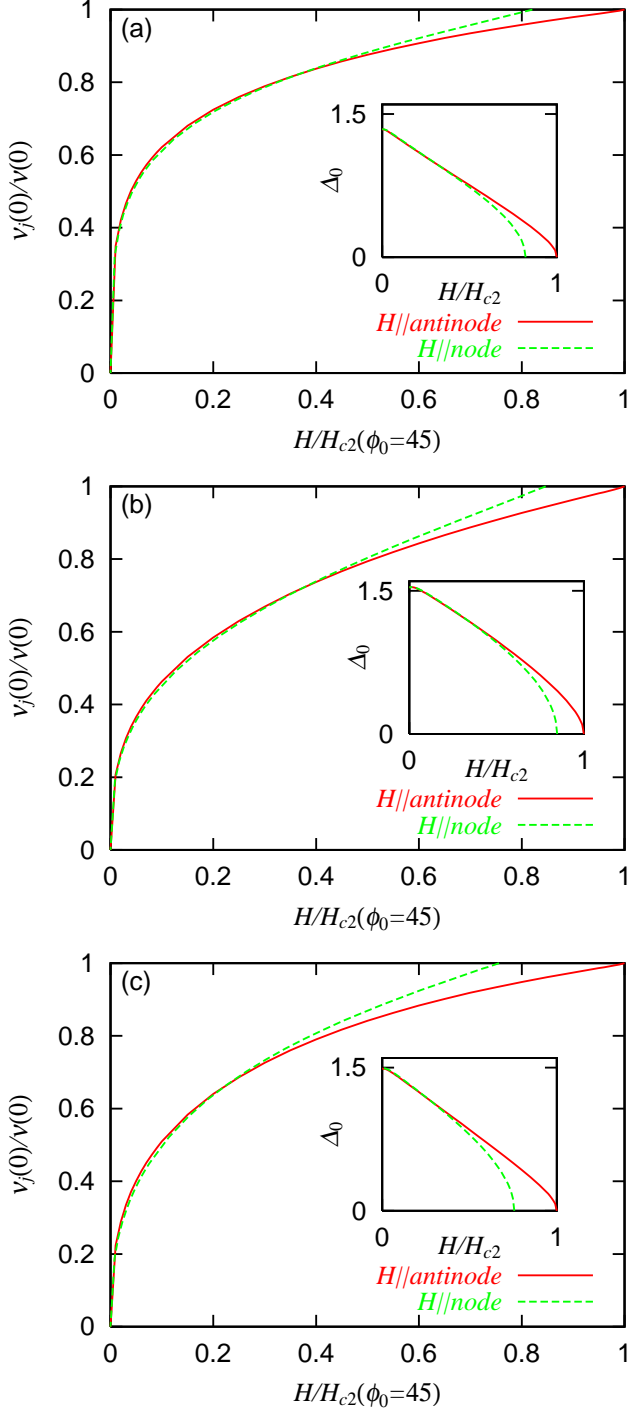


FIG. 1: Field dependence of ZEDOS under magnetic field in the nodal and antinodal directions for (a) line nodes on spherical Fermi surface, (b) line nodes on cylindrical Fermi surface, and (c) point nodes on spherical Fermi surface. (Inset) Field dependence of Δ_0 . Δ_0 is normalized with T_c , and magnetic field is normalized with H_{c2} when a field is in the antinodal direction. The agreement between (a) and the result of Eilenberger approach (fig. 4 of ref. 24) is quite good.

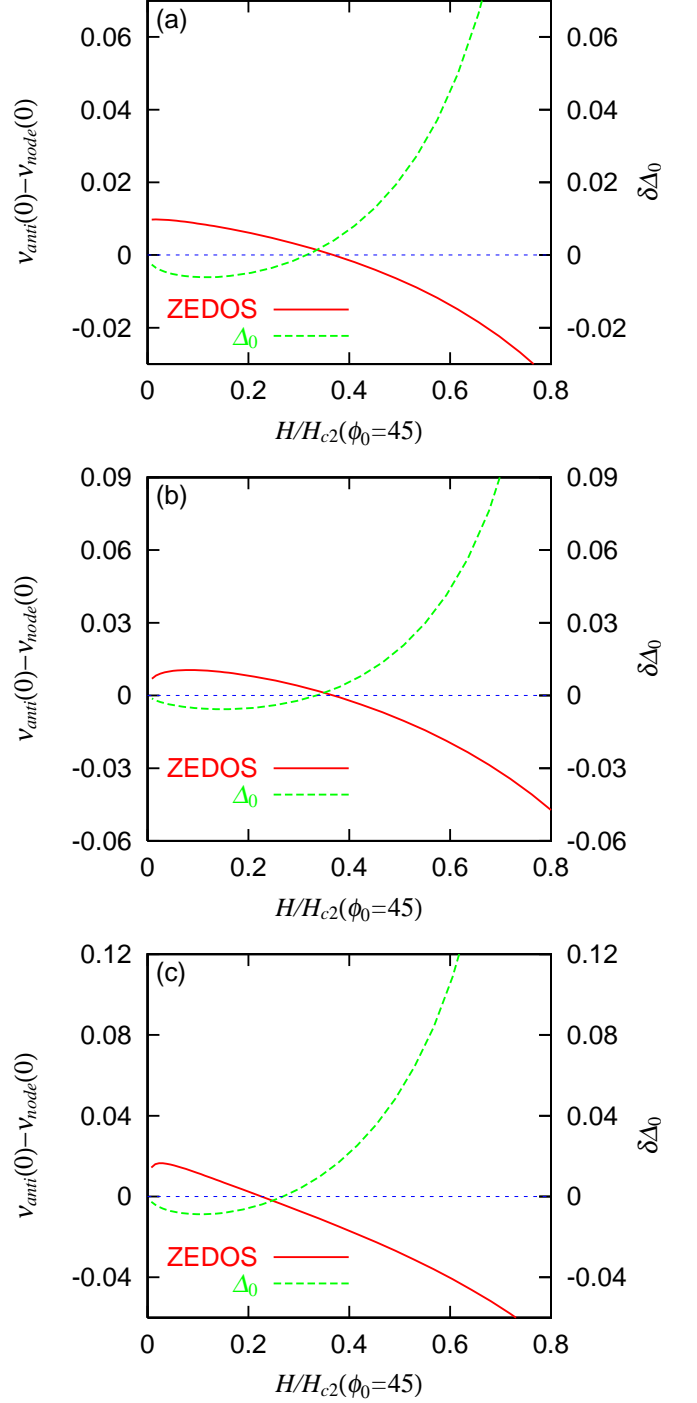


FIG. 2: Field dependence of $\delta\Delta_0$ and $\nu_{anti}(0) - \nu_{node}(0)$ for (a) line nodes on spherical Fermi surface, (b) line nodes on cylindrical Fermi surface, and (c) point nodes on spherical Fermi surface. $\delta\Delta_0$ is normalized with T_c , and magnetic field is normalized with H_{c2} when a field is in the antinodal direction.

In order to examine how the anisotropy of Δ_0 affects FODOS at low fields, we plot $\delta\Delta_0 \equiv \Delta_0(H \parallel a) - \Delta_0(H \parallel n)$ in fig. 2, together with the anisotropy of ZEDOS, $\nu_{anti}(0) - \nu_{node}(0)$. One can find that $\delta\Delta_0$ changes its sign near H^* and becomes negative for $H \lesssim H^*$. This means that anisotropy of Δ_0 has the same sign with the relation $\nu_{anti}(0) > \nu_{node}(0)$ in the Doppler-shift predominant region. Combining this with the effects of anisotropic H_{c2} at high magnetic fields, it is shown that our previous result¹² on the crossover behavior is not altered by taking account of the field-angle dependence of Δ_0 .

Next, let us study individual cases. First, let us compare the cases of line nodes on spherical Fermi surface (fig. 2(a)) and on cylindrical Fermi surface (fig. 2(b)). In spite of the difference in dimensionality of Fermi surfaces, both cases show similar behavior of $\nu_{node}(0)$ and $\nu_{anti}(0)$ with very close H^* . In fact, the small c-axis dispersion of the cylindrical Fermi surface plays a key role in this similarity. In eq. (16), information of Fermi surface is included only in $|\mathbf{v}_{F\perp}|$. In the case of cylindrical Fermi surface, $|\mathbf{v}_{F\perp}|^2 \propto \delta \cos^2(\phi - \phi_0) + \frac{1}{\delta} \epsilon^2 \sin^2 k_z$. While ϵ is much smaller than 1, one cannot neglect the term $\frac{1}{\delta} \epsilon^2 \sin^2 k_z$. In the case of anisotropic Fermi surface, one has $\delta = \frac{\xi_y}{\xi_x} \sim \sqrt{\frac{\langle v_x^2 \rangle}{\langle v_{ab}^2 \rangle}} \sim \epsilon$ in the whole range of magnetic field, as a result of minimizing the free energy eq. (5). Hence, the in-plane and the c-axis components of effective Fermi velocity, $\delta \cos^2(\phi - \phi_0)$ and $\frac{1}{\delta} \epsilon^2 \sin^2 k_z$ are scaled to be equivalent in magnitude.

Next, we study the case of point nodes on spherical Fermi surface (fig. 2(c)). In this case, one can find that the crossover field H^* is smaller ($H^* \sim 0.2H_{c2}$) than the case of line nodes ($H^* \sim 0.4H_{c2}$). This difference in H^* can be understood in terms of the shape of gap minima. To see this, we note that the reversal of the Doppler-shift criterion at high magnetic fields is caused by the quasiparticles propagating parallel to magnetic field¹². At high magnetic fields, contribution from such quasiparticles to ZEDOS, $\nu_{QP\parallel H}$, is smaller for $H \parallel a$ than $H \parallel n$, resulting in the relation $\nu_{node}(0) > \nu_{anti}(0)$. Here, for the point node case, $|\Phi(\mathbf{k}_F)|$ is quadratic near gap minima (for example, at $\theta = 90^\circ, \phi = 0^\circ$), while it is linear in the line node cases. Therefore, the order parameter is smaller near gap minima in the point node case, leading to larger $\nu_{QP\parallel H}$ for $H \parallel n$. On the other hand, there is not much difference in $\nu_{QP\parallel H}$ when $H \parallel a$. As a result, $\nu_{node}(0) - \nu_{anti}(0)$ is larger in the point node case and continues to be positive to lower field.

One may suppose that the smaller H^* can be attributed to the gap structure in the “polar part” ($\theta \sim 0^\circ$). Since in the point node case, $|\Phi(\mathbf{k}_F)| \neq 0$ except for the “equatorial part” ($\theta \sim 90^\circ$) of the Fermi surface, the effect of Doppler-shift is weaker in the “polar part”, and may lead to the smaller H^* . However, this does not hold. In fact, if we replace the gap function eq. (27) with $\Phi(\mathbf{k}_F) = \sqrt{1 - \sin^2 \theta \cos 4\phi}$, i.e., a point node model which varies linearly near gap minima, we find that $H^* \sim 0.4H_{c2}$ (fig. 3), comparable to the line node

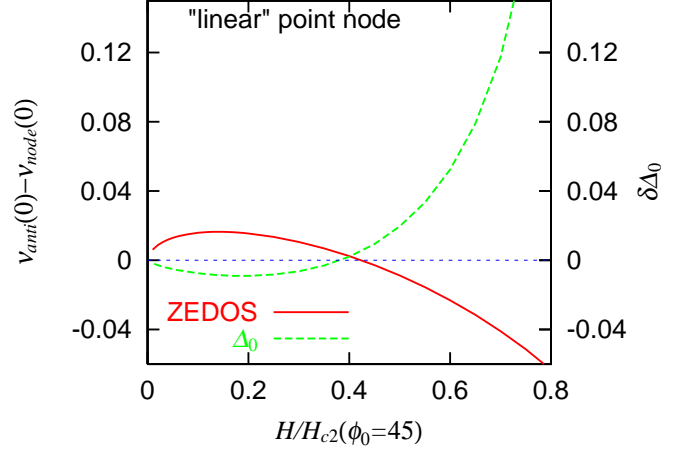


FIG. 3: Field dependence of $\delta\Delta_0$ and $\nu_{anti}(0) - \nu_{node}(0)$ for spherical Fermi surface with point nodes. Gap function is given by $\Phi(\mathbf{k}_F) = \sqrt{1 - \sin^2 \theta \cos 4\phi}$.

cases, although $|\Phi(\mathbf{k}_F)|$ is larger than the quadratic point node model (eq. (27)) everywhere on the Fermi surface.

B. Field-orientational dependence of ZEDOS

In this subsection, we study not only the amplitude but also the whole field-orientational dependence of ZEDOS. In particular, the shape of minima is of our interest, since we will discuss the origin of cusp-like minima which has been attributed to a point node in the Doppler-shift method¹³. In fig. 4, we show our results for the three models. These calculations are done at $H = 0.1H_{c2}$. One can find similar FODOS for the line node cases (fig. 4(a),(b)) with a slight difference in amplitudes. Whereas in the point node case (fig. 4(c)), one obtains FODOS with broader minima than the line node cases. Furthermore, in the point node case, tiny maxima appear when magnetic field is applied right in the nodal direction ($\phi_0 = 0^\circ$). These features again reflect the quadratic variation of order parameter near the gap minima. For comparison, we show FODOS for the gap function $\Phi(\mathbf{k}_F) = \sqrt{1 - \sin^2 \theta \cos 4\phi}$ in fig. 5, where one can find narrower minima similar to the case of line nodes. In both cases, our calculation does not support the results of Doppler-shift method.

For the better understanding of the features in FODOS, we plot contribution to FODOS from several parts of the Fermi surface in fig. 6. From these figures, one can find that FODOS is determined by the contribution from $\theta \sim 90^\circ$ on the spherical Fermi surface or $k_z \sim 0^\circ$ on the cylindrical Fermi surface. In other words, Most contribution comes from the part where effective Fermi velocity $\mathbf{v}_{F\perp}$ (eq. (14)) is parallel to the field-rotational plane. One can coherently understand the features of FODOS and H^* obtained in this section from this viewpoint.

First, the difference between point node and line node

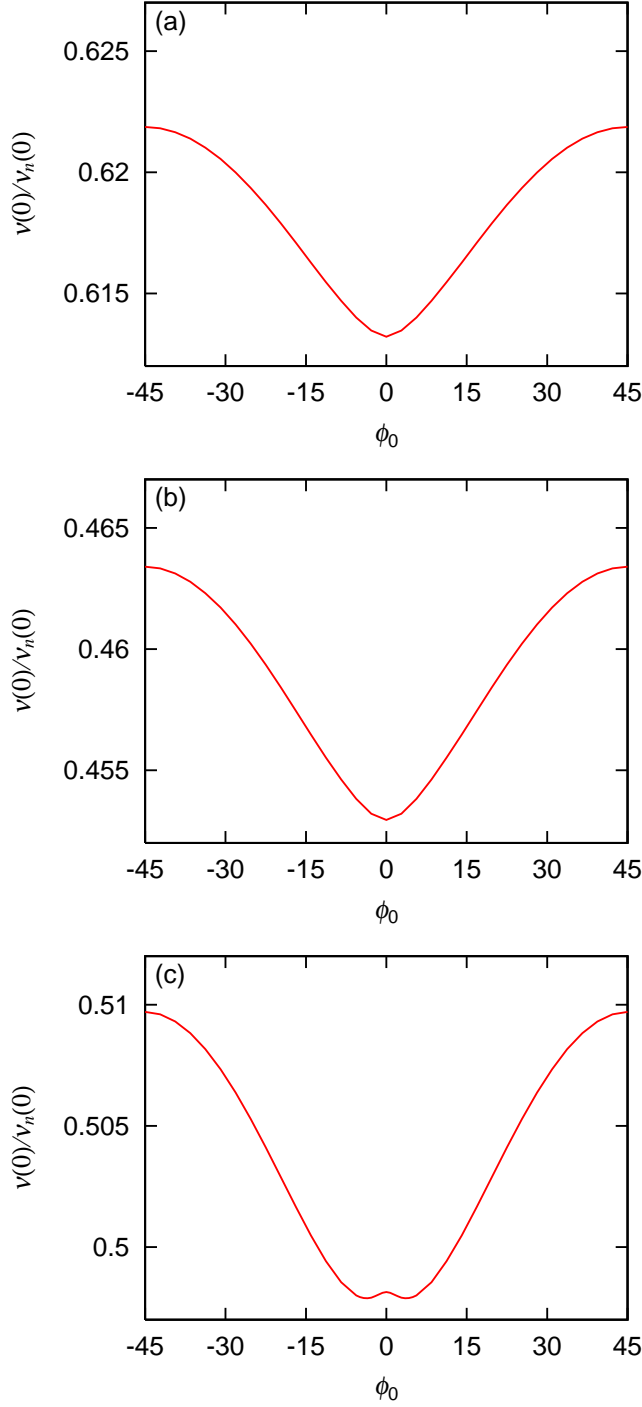


FIG. 4: Field-orientational dependence of ZEDOS for (a) line nodes on spherical Fermi surface, (b) line nodes on cylindrical Fermi surface, and (c) point nodes on spherical Fermi surface.

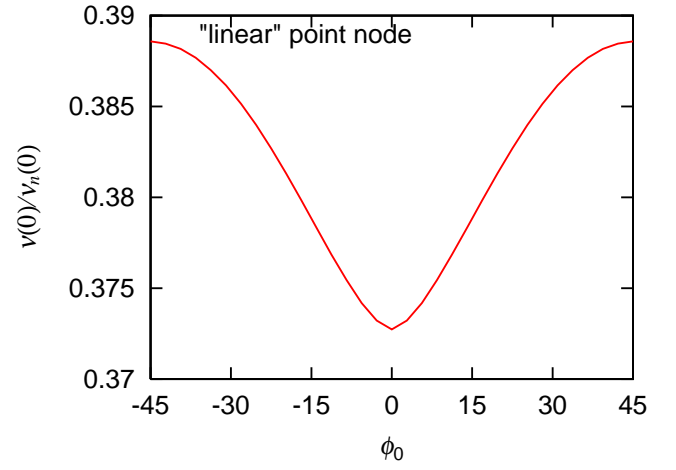


FIG. 5: Field-orientational dependence of ZEDOS for (a) spherical Fermi surface with point nodes. Gap function is given by $\Phi(\mathbf{k}_F) = \sqrt{1 - \sin^2 \theta \cos 4\phi}$.

is unimportant, because these gap structures behave similarly at $\theta \sim 90^\circ$, where $\mathbf{v}_{F\perp}$ is parallel to the field-rotational plane. The dimensionality of Fermi surface is also unimportant. While Fermi velocity is almost parallel to the field-rotational plane on a cylindrical Fermi surface, the effective Fermi velocity is so only near $k_z \sim 0^\circ$, due to small $\delta(\sim \epsilon)$. Whereas it is important whether order parameter varies linearly or quadratically near gap minima, because this difference lies in $\theta \sim 90^\circ$. In this sense, H^* and FODOS are determined by the local structure of order parameter on the part where $v_{F\perp}$ is parallel to the field-rotational plane, rather than the global nodal structure of the entire Fermi surface.

IV. EFFECTS OF IN-PLANE ANISOTROPY OF FERMION SURFACE

In this section, we examine the effects of in-plane anisotropy of Fermi surface on FODOS. The anisotropy of Fermi surface affects ZEDOS through $|\mathbf{v}_{F\perp}|$ in eq. (16). If the distribution of $|\mathbf{v}_{F\perp}|$ changes according to the magnetic field direction, ZEDOS also depends on the field direction, even without gap nodes. In this section, we focus on the shift of H^* with increasing anisotropy of Fermi surface.

In order to take account of the in-plane anisotropy of Fermi surface, we consider a simplified model shown in fig. 7. We make Fermi surface by connecting the sets of wave numbers, i.e. by adding nested parts to a cylindrical Fermi surface.

$$(k_a, k_b) = (\pm(u+v), k_b), \quad (-v < k_b < v), \quad (29)$$

$$(k_a, k_b) = (k_a, \pm(u+v)), \quad (-v < k_a < v), \quad (30)$$

$$(k_a, k_b) = (\pm v \pm u \cos \phi, \pm v \pm u \sin \phi), \quad (0 < \phi < \frac{\pi}{2}) \quad (31)$$

Here, $\zeta = v/u$ is a measure of anisotropy. When $\zeta = 0.5$ and 1.0, the linear parts occupy 24.1 and 38.9% of the Fermi surface, respectively.

We assume the absolute value of in-plane components of Fermi velocity v_F are the same all over the Fermi surface, and set a c-axis component $v_{Fc} = 0.05v_F \sin k_z$. We assume a $d_{x^2-y^2}$ -like pairing, i.e.

$$\Phi(\mathbf{k}_F) \propto \cos(2 \tan^{-1}(\frac{k_b}{k_a})), \quad (32)$$

i.e., gap nodes are on the cylindrical parts of the Fermi surface.

When magnetic field is applied perpendicular to one of the nested parts, $|\mathbf{v}_{F\perp}| \sim 0$ on the nested parts, leading to suppression of ZEDOS. Whereas, when magnetic field is applied in the nodal direction, the nested parts does not influence ZEDOS so much. Hence, it is expected that

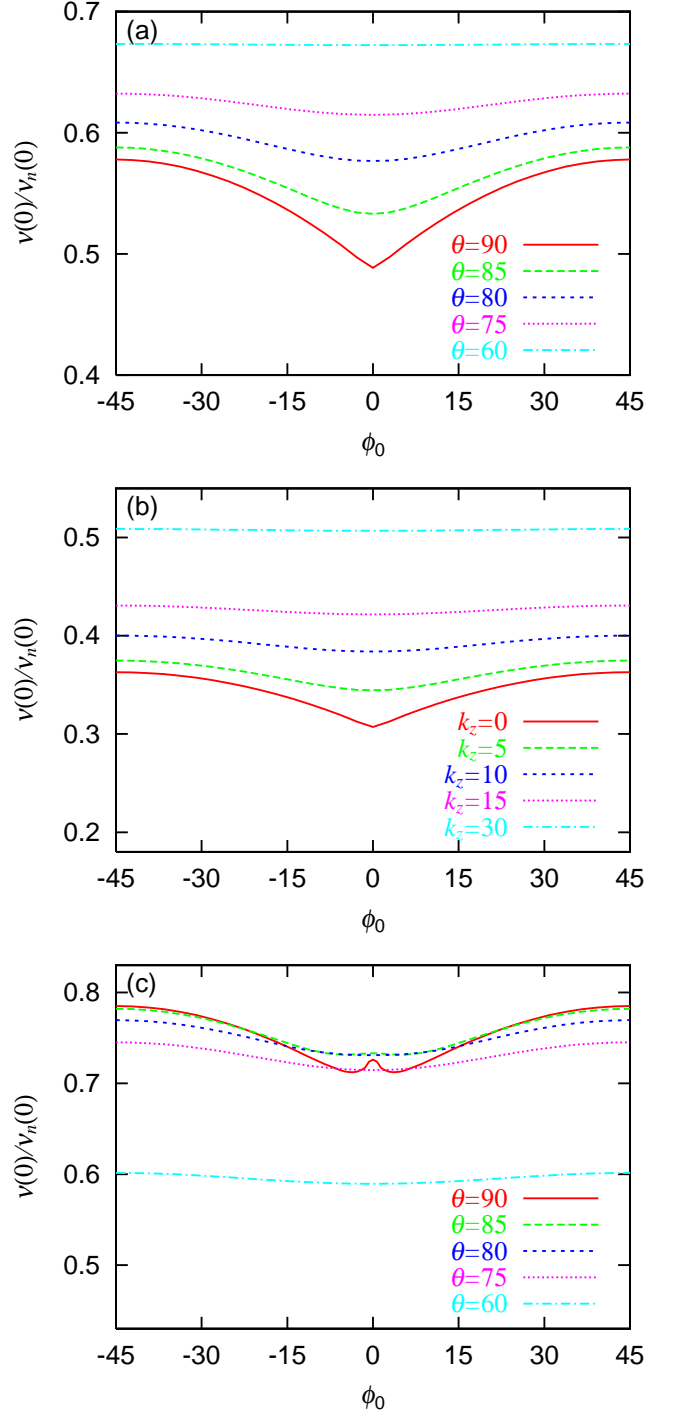


FIG. 6: Contribution to FODOS from several parts of the Fermi surface for (a) line nodes on spherical Fermi surface, (b) line nodes on cylindrical Fermi surface, and (c) point nodes on spherical Fermi surface. In these three cases, total FODOS is given by averaging over θ ($0^\circ < \theta < 90^\circ$) or k_z ($-\pi < k_z < \pi$).

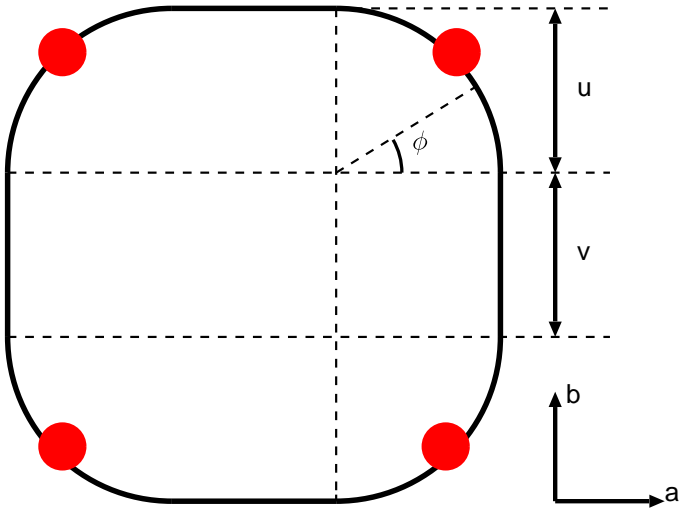


FIG. 7: A schematic picture of the Fermi surface with in-plane anisotropy seen from the c -axis. Position of gap node is shown with filled circles

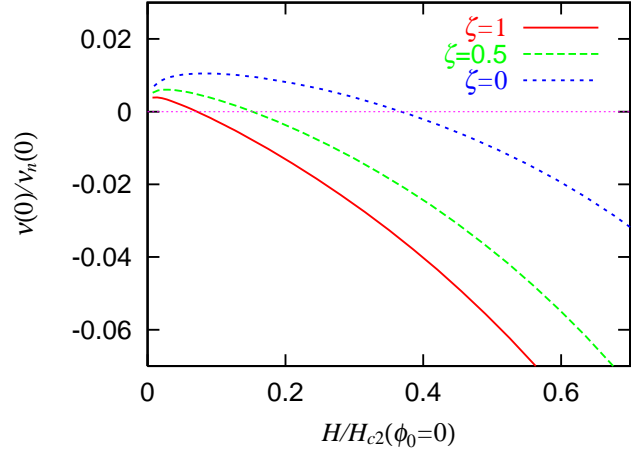


FIG. 8: Comparison of $\nu_{node}(0)$ and $\nu_{anti}(0)$ for $\zeta = 0, 0.5, 1.0$. Magnetic field is normalized with H_{c2} when a field is in the antinodal direction.

the Doppler-shift predominant region is suppressed as ζ is increased. In fig. 8, we show $\nu_{anti}(0) - \nu_{node}(0)$ for several values of ζ . One can find that H^* is lowered as ζ is increased. At $\zeta = 1.0$, the Doppler-shift predominant region is suppressed to $H \sim 0.05H_{c2}(\phi_0 = 45^\circ)$, i.e., the almost entire field range at which experiments have been done.

This result suggests that many cares should be taken to apply the “Doppler-shift criterion” when Fermi surface is highly anisotropic. At least one should check that maxima and minima of FODOS are exchanged at high fields and low fields, in order to confirm that the system enters the Doppler-shift predominant region at low magnetic fields. It seems that recent experiments do not find any exchange of maxima and minima^{5,6}.

V. ORIGIN OF THE CUSP-LIKE SINGULARITY

In this section, we study origin of the cusp-like singularity in FODOS observed through specific heat⁹ and thermal conductivity⁸ in $\text{YNi}_2\text{B}_2\text{C}$. In both cases, the cusp-like minima are observed when magnetic field is applied parallel to a or b -axis. So far, the cusp-like minima are attributed to point nodes on the superconducting gap. In particular, $s+g$ -wave gap structure has been proposed for $\text{YNi}_2\text{B}_2\text{C}$ ¹³. However, as we showed in section III, rather broader minima of FODOS are obtained from $s+g$ -wave-like quadratic point nodes.

Here, we would like to propose a new mechanism that leads to cusp-like minima in FODOS. In our theory, two conditions are required for the appearance of cusp-like minima. The first condition is that a system has to have a quasi-two-dimensional nested Fermi surface. And the second condition is that the superconducting coherence lengths are isotropic. Under these conditions, cusp-like

minima appear when a magnetic field is applied perpendicular to the nested part of the Fermi surface.

Here, we briefly describe how cusp-like minima appear from the above conditions, in terms of eq. (16). Provided that superconducting coherence lengths are isotropic, one obtains $\delta = \frac{\xi_c}{\xi_a} \sim 1$. When the magnetic field is applied at an angle ϕ_0 with the normal line of the nested part of the Fermi surface, we have

$$|\mathbf{v}_{F\perp}|^2 = v_F^2 (\sin^2 \phi_0 + \epsilon^2 \sin^2 k_z). \quad (33)$$

on the nested part, with a c-axis component of Fermi velocity, $\epsilon \sin k_z$. If the c-axis dispersion is weak enough ($\epsilon \ll 1$), one can ignore the second term in the right-hand side, and the contribution to ZEDOS from the nested part of the Fermi surface $\nu_{nest}(0)$ is written as

$$\begin{aligned} \nu_{nest}(0) &\propto \frac{1}{\sqrt{1 + \frac{2\Lambda}{\pi^2} |\Delta_0|^2 \left(\frac{|\Phi(\mathbf{k}_F)|}{v_F \sin \phi_0} \right)^2}} \\ &\sim \frac{\pi v_F}{\sqrt{2\Lambda} |\Delta_0 \Phi(\mathbf{k}_F)|} |\sin \phi_0|, \end{aligned} \quad (34)$$

for small ϕ_0 . Hence, FODOS has cusp-like minima at $\phi_0 = 0$, i.e., when a magnetic field is applied perpendicular to the nested parts.

The $|\sin \phi_0|$ dependence in eq. (34) allows one a simple physical interpretation. Suppose a quasiclassical trajectory^{34,35,36} of nested Fermi surface, which is running in the direction at an angle ϕ_0 with magnetic field, and passing near vortex cores (fig. 9). On this trajectory, phase of order parameter changes drastically near vortex cores, leading to formation of Andreev bound states. Since the vortex cores are separated by the distance $\sim \frac{\sqrt{\Lambda}}{|\sin \phi_0|}$ on the trajectory, the density of Andreev bound states is proportional to $\frac{|\sin \phi_0|}{\sqrt{\Lambda}}$, hence make a cusp-like singularity in FODOS. This brief discussion reveals that the cusp-like singularity is caused by the core states, which are not properly taken into account in the Doppler-shift method.

Here, we discuss the basic properties of $\text{YNi}_2\text{B}_2\text{C}$. $\text{YNi}_2\text{B}_2\text{C}$ has three bands (17th, 18th, 19th) crossing Fermi energy^{25,26,27}. The 17th band, which mainly consists of Ni(4d) orbits, forms an open Fermi surface in the c-axis direction, hence has a quasi-two-dimensional nature^{25,26,27}. It is reported that the corresponding Fermi surface of $\text{LuNi}_2\text{B}_2\text{C}$ has a nested part, with nesting vectors $\mathbf{q} \sim (0.56 \times 2\pi)\mathbf{e}_a, (0.56 \times 2\pi)\mathbf{e}_b$ ²⁷. Kohn anomaly in phonon spectrum^{28,29,30} provides another evidence of the nesting. On the other hand, the 18th and the 19th bands form closed Fermi surface in the c-axis direction, hence have three-dimensional tendency. As to the gap structure, existence of nodes have been confirmed by specific heat³¹ and ultra-sonic attenuation³² etc.

In order to discuss the features of $\text{YNi}_2\text{B}_2\text{C}$, we study the following two-band model. Our model consists of (α) a partly nested quasi-two-dimensional Fermi surface as shown in fig. 7, and (β) a three-dimensional

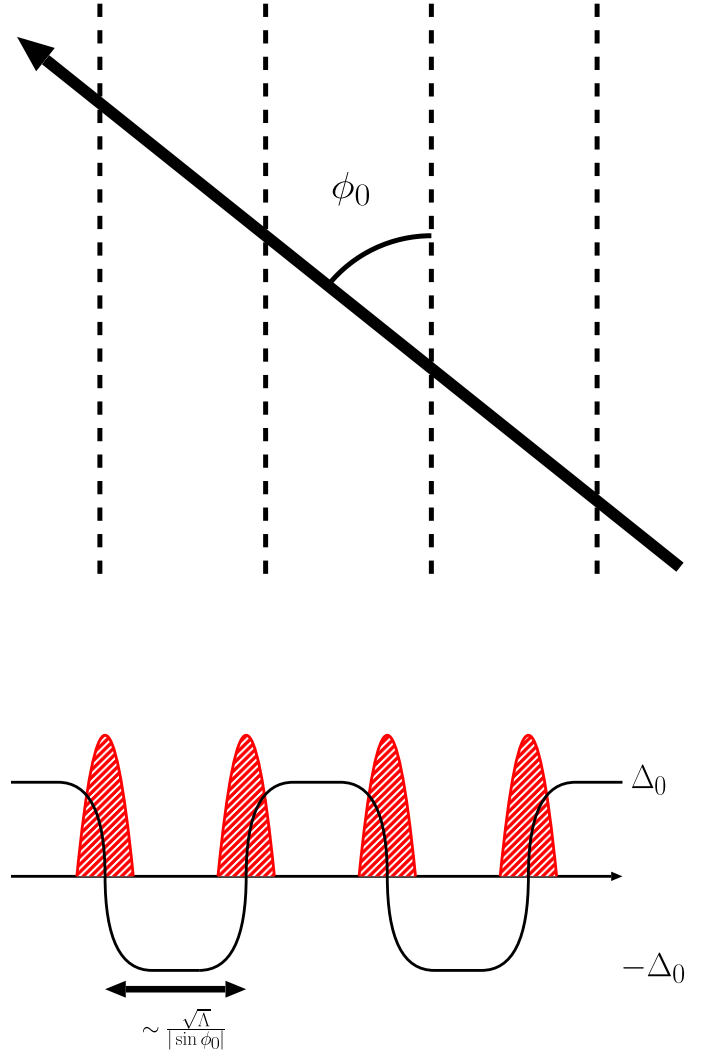


FIG. 9: (upper) A schematic picture of a trajectory running at an angle ϕ_0 with magnetic field. Vortex cores are shown with dashed lines. (lower) Andreev bound states formed on the trajectory.

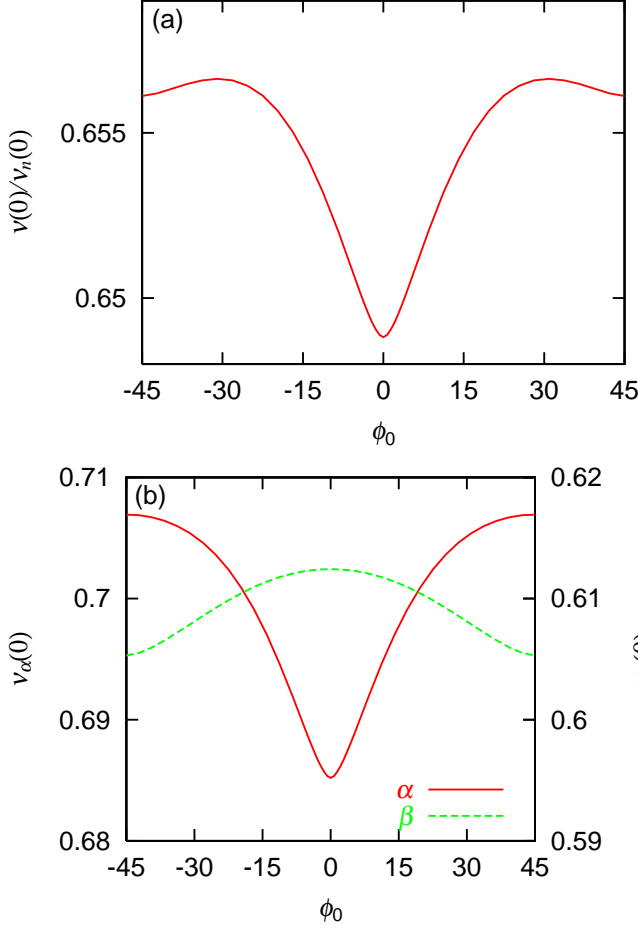


FIG. 10: (a) FODOS of the two-band model. Gap function (i) is adopted for the nodal structure of the spherical Fermi surface. (b) Contribution to FODOS from each Fermi surface.

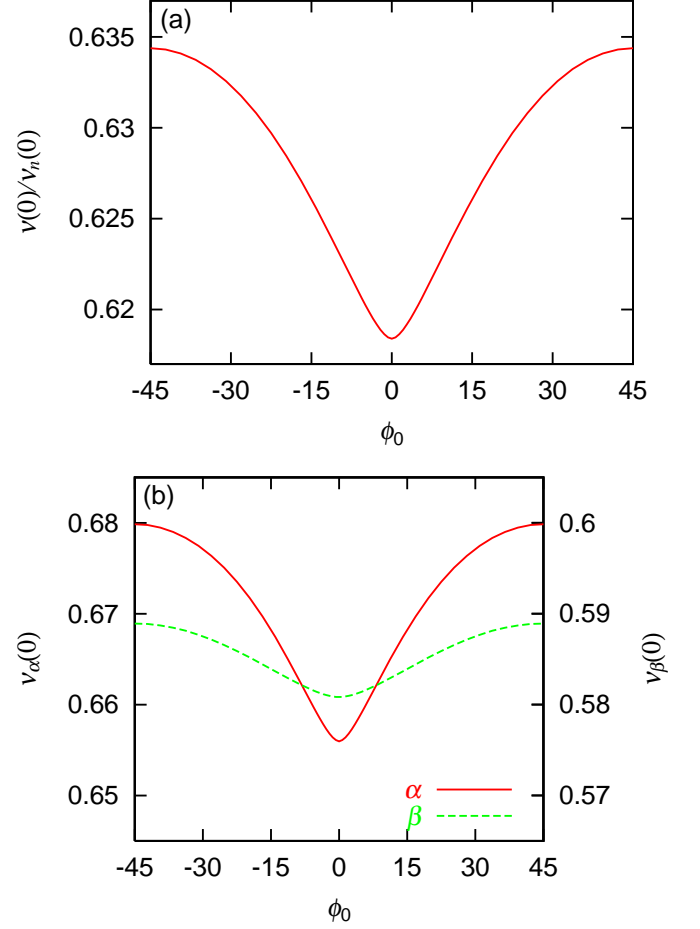


FIG. 11: (a) FODOS of the two-band model. Gap function (ii) is adopted for the nodal structure of the spherical Fermi surface. (b) Contribution to FODOS from each Fermi surface.

spherical Fermi surface. We suppose the normal-state density of states of these two Fermi surfaces are the same. We set $\zeta = v/u = 0.137$ for the first Fermi surface. Then, about 4% of the entire Fermi surfaces are nested, in agreement with ref. 27, where the proportion of the nested part is reported to be $4.4 \pm 0.5\%$. As to the gap structure, we assume isotropic gap for the quasi-two-dimensional Fermi surface, and the following two cases for the spherical Fermi surface, with different nodal position: (i) $\Phi(\mathbf{k}_F) = \sqrt{\frac{15}{4}} \sin^2 \theta \sin 2\phi$ and (ii) $\Phi(\mathbf{k}_F) = \sqrt{\frac{15}{4}} \sin^2 \theta \cos 2\phi$. As to the interaction potential $V^{\alpha\beta}$ in eq. (21), we assume $V^{\alpha\beta}/V^{\alpha\alpha} = 0.5$ and $V^{\beta\beta}/V^{\alpha\alpha} = 3.0$. Here, we assume spherical Fermi surface has the larger superconducting instability, in order to make superconducting coherence lengths of this system isotropic³³.

In fig. 10(a) and fig. 11(a), we give FODOS of this model. Calculation is done at $H = 0.1H_{c2}(\phi_0 = 0^\circ)$. One can find a clear cusp-like minima in both cases. Furthermore, it is worth noting that FODOS has minima for

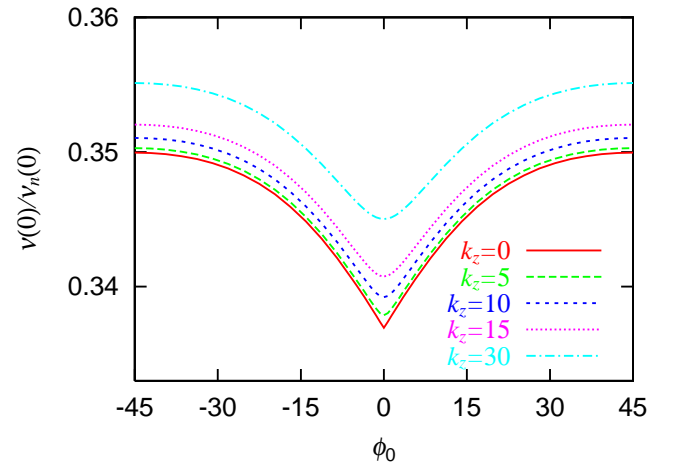


FIG. 12: Contribution to FODOS from several k_z of the quasi-two-dimensional Fermi surface. This figure should be compared with fig. 6(b)

$H \parallel a(\phi_0 = 0)$, irrespective of the nodal position. In fig. 10(b) and fig. 11(b), we show contribution to FODOS from each Fermi surface. One can find that the FODOS arising from the quasi-two-dimensional Fermi surface is larger and dominates the contribution from the spherical Fermi surface. It is surprising that only tiny anisotropy of Fermi surface destroys the Doppler-shift predominant region below $H = 0.1H_{c2}(\phi_0 = 0^\circ)$. It makes a contrast with the single band case in section IV where as much as 40% of Fermi surface has to be nested to suppress the Doppler-shift predominant region to $H \sim 0.05H_{c2}$.

One can understand the origin of the enhancement of the contribution from the quasi-two-dimensional Fermi surface, on the basis of the scenario in section III. In section III, we noted that largest contribution to FODOS comes from the part of Fermi surface where effective Fermi velocity $\mathbf{v}_{F\perp}$ is nearly parallel to the field-rotational plane. In the case of cylindrical Fermi surface in section III, such parts are limited to $k_z \sim 0$ due to anisotropic coherence lengths $\delta \sim \epsilon$. However, in the two-band model in this section, the superconducting coherence lengths are isotropic ($\delta \sim 1$), hence $\mathbf{v}_{F\perp}$ is almost parallel to the field-rotational plane all over the quasi-two-dimensional Fermi surface. Therefore, contribution to FODOS come from all k_z and becomes much larger than the contribution from the nodal structure on the spherical Fermi surface. We plot contribution to FODOS from several k_z in fig. 12. In this figure, one can find that all k_z contribute to FODOS equally.

The cusp-like singularity shown here is basically owing to the co-existence of two-dimensional and three-dimensional Fermi surfaces and to the nesting nature of two-dimensional Fermi surface. This example shows that many cares are needed for an analysis of experimental data in the multi-band system. Then, anisotropy of quasi-two-dimensional Fermi surface is enhanced and invalidates the simple argument based on the Doppler-shift methods.

VI. CONCLUSIONS

We study the influence of superconducting gap and Fermi surface structures on the field-orientational depen-

dence of ZEDOS. First, we studied the crossover behavior of ZEDOS, by taking account of the four-fold oscillation of Δ_0 , and found that there exists a crossover magnetic field H^* so that $\nu_{anti}(0) > \nu_{node}(0)$ for $H < H^*$, while $\nu_{node}(0) > \nu_{anti}(0)$ for $H > H^*$, consistent with our previous analyses¹².

Next, we have investigated the roles of gap structure and nature of Fermi surface. The crossover behavior and FODOS at the Doppler-shift predominant region have been discussed. We found that there are no significant differences in neither the value of H^* nor the shape of FODOS between the spherical Fermi surface and the cylindrical Fermi surface, in spite of the difference in the dimensionality of Fermi surface. We also found that when quadratic point nodes exist, H^* is lowered than the line node cases and FODOS has broader minima. These results can be coherently understood by recognizing that contribution to FODOS mostly comes from the part on the Fermi surface where effective Fermi velocity is nearly parallel to the field-rotational plane.

Next, we examine the effects of in-plane anisotropy of Fermi surface. We showed that the Doppler-shift predominant region may be suppressed to lower fields by the anisotropy of Fermi surface. This tendency becomes especially strong in a multi-band superconductor which has nearly isotropic coherence lengths. Therefore, some cares are necessary for analyzing the field-rotational experiments for $\text{YNi}_2\text{B}_2\text{C}$ and CeCoIn_5 . On the other hand, the field-rotational experiment and its interpretation based on the Doppler-shift criterion are powerful tool for such material as Sr_2RuO_4 , $\text{Na}_{0.35}\text{CoO}_2 \cdot 1.3\text{H}_2\text{O}$ ³⁷ and organic superconductors, which are well described by a single Fermi surface or have plural Fermi surfaces with the same dimensionality.

Finally, we propose a novel mechanism of the cusp-like minima found in $\text{YNi}_2\text{B}_2\text{C}$, in terms of Andreev bound states. The cusp-like minima are attributed to nesting in quasi-two-dimensional Fermi surface and the isotropy of superconducting coherence lengths.

We are grateful to Y. Matsuda, T. Sakakibara, Y. Kato, K. Izawa, H. Kusunose and T. Watanabe for fruitful discussions. We would also like to thank K. Kamata for providing her master thesis on the field-rotational experiments of $\text{YNi}_2\text{B}_2\text{C}$.

-
- ¹ K. Izawa, H. Takahashi, H. Yamaguchi, Yuji Matsuda, M. Suzuki, T. Sasaki, T. Fukase, Y. Yoshida, R. Settai, and Y. Onuki, Phys. Rev. Lett **86**, 2653 (2001).
 - ² M. A. Tanatar, M. Suzuki, S. Nagai, Z. Q. Mao, Y. Maeno, and T. Ishiguro, Phys. Rev. Lett **86**, 2649 (2001).
 - ³ K. Deguchi, Z. Q. Mao, H. Yaguchi, and Y. Maeno, Phys. Rev. Lett. **92**, 047002 (2004).
 - ⁴ K. Deguchi, Z. Q. Mao and Y. Maeno, J. Phys. Soc. Jpn. **73**, 1313 (2004).
 - ⁵ K. Izawa, H. Yamaguchi, Yuji Matsuda, H. Shishido, R. Settai, and Y. Onuki, Phys. Rev. Lett **87**, 057002 (2001).

- ⁶ H. Aoki, T. Sakakibara, H. Shishido, R. Settai, Y. Onuki, P. Miranović, and K. Machida, J. Phys.: Condens. Matter **16**, No 3, (2004) L13-L19.
- ⁷ K. Izawa, H. Yamaguchi, T. Sasaki, and Yuji Matsuda, Phys. Rev. Lett **88**, 027002 (2002).
- ⁸ K. Izawa, K. Kamata, Y. Nakajima, Y. Matsuda, T. Watanabe, M. Nohara, H. Takagi, P. Thalmeier, and K. Maki Phys. Rev. Lett **89**, 137006 (2002).
- ⁹ Tuson Park, M. B. Salamon, Eun Mi Choi, Heon Jung Kim, and Sung-Ik Lee Phys. Rev. Lett **90**, 177001 (2003).
- ¹⁰ K. Izawa, Y. Nakajima, J. Goryo, Y. Matsuda, S. Osaki,

- H. Sugawara, H. Sato, P. Thalmeier, and K. Maki Phys. Rev. Lett **90**, 117001 (2003).
- ¹¹ T. Watanabe, K. Izawa, Y. Kasahara, Y. Haga, Y. Onuki, P. Thalmeier, K. Maki and Y. Matsuda, cond-mat/0405211
 - ¹² M. Udagawa, Y. Yanase, and M. Ogata, cond-mat/0401206.
 - ¹³ P. Thalmeier and K. Maki, cond-mat/0210364.
 - ¹⁴ W. Pesch, Z. Phys. B **21**, 263 (1975); P. Klimesch and W. Pesch, J. Low Temp. Phys. **32**, 869 (1978).
 - ¹⁵ T. Dahm, S. Graser, C. Iniotakis, and N. Schopohl, Phys. Rev. B **66**, 144515 (2002).
 - ¹⁶ S. Graser, T. Dahm, and N. Schopohl, Phys. Rev. B **69**, 014511 (2004).
 - ¹⁷ H. Kusunose, cond-mat/0401077.
 - ¹⁸ L. Tewordt and D. Fay, Phys. Rev. B **64**, 024528 (2001).
 - ¹⁹ G. Eilenberger, Z. Phys., **214**, 195 (1968).
 - ²⁰ A. I. Larkin and Y. N. Ovchinnikov, Sov. Phys. JETP **46**, 155 (1977).
 - ²¹ U. Klein, J. Low. Temp. Phys. **69**, 1 (1987).
 - ²² N. Schopohl, J. Low Temp. Phys. **41**, 409 (1980).
 - ²³ T. Dahm and N. Schopohl, Phys. Rev. Lett **91**, 017001 (2003).
 - ²⁴ P. Miranović, N. Nakai, M. Ichioka, and K. Machida, Phys. Rev. B **68**, 052501 (2003).
 - ²⁵ J. I. Lee, T. S. Zhao, I. G. Kim, B. I. Min, and S. J. Yoon, Phys. Rev. B **50**, 403 (1994).
 - ²⁶ D. J. Singh, Solid State Commun. **49**, 899 (1996).
 - ²⁷ S. B. Dugdale, *et al.*, Phys. Rev. Lett. **83**, 4824 (1999).
 - ²⁸ P. Dervénagas, M. Bullock, J. Zarestky, P. Canfield, B. K. Cho, B. Harmon, A. I. Goldman, and C. Stassis, Phys. Rev. B **52**, R9839 (1995)
 - ²⁹ H. Kawano, H. Yoshizawa, H. Takeya, and K. Kadowaki, Phys. Rev. Lett. **77**, 4628 (1996).
 - ³⁰ C. Stassis, M. Bullock, J. Zarestky, P. Canfield, A. I. Goldman, G. Shirane and S. M. Shapiro, Phys. Rev. B **55**, R8678 (1997).
 - ³¹ M. Nohara, M. Isshiki, F. Sakai and H. Takagi, J. Phys. Soc. Jpn., **68**, 1078 (1999).
 - ³² T. Watanabe, M. Nohara, T. Hanaguri, and H. Takagi, Phys. Rev. Lett. **92**, 147002 (2004).
 - ³³ H. Takagi, M. Nohara and R. J. Cava, Physica B, **237-238**, 292 (1997).
 - ³⁴ J. W. Serene and D. Rainer, Phys. Rep. **101**, 221 (1983).
 - ³⁵ N. Kopnin, *Theory of Nonequilibrium Superconductivity*.
 - ³⁶ N. Schopohl, cond-mat/9804064.
 - ³⁷ K. Takada, H. Sakurai, E. Takayama-Muromachi, F. Izumi, R. A. Dilanian and T Sasaki, Nature **422**, 53 (2003).